

Enhancing Wireless Communication: Design and Analysis of Ultra-Wideband Fork Monopole Antenna with Substrate Integrated Waveguide Resonator

Roger Merriman^{1*} and Khaled Bawaneh²

¹ Department of Industrial Engineering, Wichita State University, Kansas, USA.

² School of Business, Clark Atlanta University, Georgia, USA.

Received: 27 Jul. 2024, Revised: 2 Aug. 2024, Accepted: 5 Aug. 2024.

Published online: 1 Sep. 2024.

Abstract: The fast growth of wireless communication across networks and devices, driven by IoT, forced the antennas to be compact, light, less expensive, and high-performing ones that meet the required market expectations and optimize the wireless systems. Hence, these antenna types can be considered options to overcome the mentioned difficulties. The following research offers a concept of a UWB fork monopole antenna with a substrate-integrated waveguide resonator for further use. Applying a based antenna improves antenna efficiency, wider bandwidth, with less dimension and weight. We have developed a particular antenna prototype to measure and verify this methodology. The connection of adding array holes to the antenna in its bandwidth properties will be considered. The results bring a level of knowledge about using a Swiss roll-based antenna in wireless communication designing and optimization, providing valuable information concerning enhancing performance and efficiency to overcome the dynamic IoT challenges.

Keywords: SIW, impedance matching, microstrip components, square patch, microstrip line feeding.

1 Introduction

With the rise of wireless communication technologies and their extensive use, such as 5G networks, IoT devices, and medical imaging, the growing demand for easy-to-use, large quantity manufacturing, affordable, and more efficient antennas has emerged. The patch antenna, or precisely, "Microstrip," is the most preferred solution. It has an integrated circuit board (ICB) based design and takes a flat geometry like rectangular, circular, or triangle, which are only examples [1-4]. Patch antennas typically comprise a single layer of thin copper foil, coated with a corrosion-resistant metal such as gold, tin, or nickel. Falling under the category of single-element resonant antenna designs, they consist of four primary components: the patch, ground plane, substrate, and feeding part. The patch, often a skinny metal strip or an array of strips, is situated on one side of a thin, non-conducting substrate—a dielectric material like FR4 Epoxy—where the thickness (t) is significantly smaller than the free space wavelength (λ_0) [5-7]. The ground plane, also made of the same metal, is positioned on the opposite side of the substrate, completing the structure and enabling efficient electromagnetic wave propagation.

The production of patch antennas involves a straightforward and cost-effective process. The compact size of the entire structure results in minimal material consumption, thereby reducing the overall manufacturing cost of the antenna. Thus, the advantages of patch antennas can be summarized as follows:

- Wide variety of applications.
- Simple and small circuit.
- Low cost.

Patch antennas possess a directive beam, enabling the majority of the gain to be transmitted and concentrated within a narrow area, facilitating clear transmission and extending the reach to farther distances. They also offer a reasonably wide bandwidth for various applications, particularly wireless and mobile communication. Primarily functional in the microwave range (1GHz - 300GHz), patch antennas benefit from short wavelengths, providing a high penetration ability that grants the signal immunity to losses and distortion [8].

Efforts to achieve compact antenna structures have explored fractal geometries. Although fractal antenna shapes result in advantageous downsizing outcomes, their mechanical restrictions make producing these structures

*Corresponding author e-mail: roger.merriman@wichita.edu

challenging. Substrate integrated waveguide resonators have recently come to light as a viable remedy for the problems associated with antenna downsizing. To combine the advantages of both planar and nonplanar structures—such as waveguides, microstrip lines, and rectangular antenna patches—substrate-integrated waveguides (SIW) can be smoothly incorporated into both structures [9–12]. Additionally, the invention of the SIW technique has led to the extended field of regular microwave waveguides or resonators with high-quality factors via exploiting the metalized vias or dielectric substrate cavities. Conventional microstrip circuits provide the advantages of being low-cost, easy-to-manufacture, and small-size, which are still present in SIW, but now they also offer the benefit of having high-quality factor, which in the meantime, was only possible to achieve with expensive metallic waveguides, that are also large.

In an inductive post design, especially for microwave filters, the proliferation of passive Substrate Integrated Waveguide (SIW) components has recently been discovered as a remarkable improvement. This integration scheme has been contemplated as a preliminary step aimed at achieving an impressive increase in the Q-factor over conventional microstrip implementation. Likewise, the series of SIW packets has laid the basis for chipless Radio Frequency Identification (RFID) tags, showing that standoff wave cavities are the right choice. From the recent experimental experiments that have been carried out, it has been proven that the application of SIW technology dramatically improves the efficiency and performance of the devices.

The concluding step is the fabrication of a compact, cost-effective prototype that possesses this functionality by limited space, reasonable price, and superior performance in the broad spectrum of frequencies. This prototype simulates antenna design and optimization transformation to their professional implementation level. It uses the modified PSO as the basis for optimization of the antenna pattern.

The paper provides a detailed explanation of the recommended antenna design and evaluation procedure. It outlines the proposed methods, including the PSO approach to iterative optimization and the critical components needed for antenna performance. The research then conducts a prototype using the procedure, verified through practical testing and numerical simulations. The research outcomes, facilitating study interpretation, and proposing ideas for further investigation. It provides a clear understanding of the proposed research's meaning of antenna design and improvement and highlights the importance and prospects of the suggested methodology.

Antenna Design

There are a few parameters that must be put into consideration when designing a patch antenna:

1. The desired fundamental frequency (f_0)
2. Thickness of the substrate layer (h_0)
3. Type of dielectric material and its relative permittivity (ϵ_r)

The substrate selection is crucial for designing a microstrip patch antenna, as depicted in Figure 1. Without proper consideration of substrate parameters such as length, width, height, and dielectric constant, achieving optimal antenna performance is challenging. Materials like FR4, PTFE, and RT droid 5880 are commonly used substrates chosen based on specific requirements and desired performance characteristics. The feeding line plays a significant role in antenna performance at high signal frequencies. Careful design of the antenna feeding is essential to ensure correct impedance matching and overall antenna effectiveness [16-18].

A feeding line's impedance should match the patch's properties for optimal outcomes.

Figure 2 reports the structure of the UWB antenna. A fork monopole antenna with a microstrip feeding line of width F is proposed in the paper. The ground plane, which comprises a copper strip with height and breadth of $\epsilon_r = 4.4$ with height $h=0.8mm$, is printed on the rear side of the dielectric substrate, FR4 epoxy. The fork monopole is backed by a surface-integrated waveguide SIW cavity enabled by several metalized vias. The goal of the SIW cavity is to increase antenna performance concerning S_{11} return loss [19–22]. Referring to the figure.2.2 The SIW cavity has sixteen metalized holes with a diameter less than D , with a S_4 inter-element hole spacing.

The design process is accomplished by applying the following steps:

Step 1: Width of the patch (W_p) calculation:

$$W_p = \frac{c}{2f_0 \sqrt{\frac{\epsilon_r + 1}{2}}} \quad (1)$$

Step 2: Effective dielectric constant (ϵ_{eff}) calculation

$$\epsilon_{\text{eff}} = \frac{\epsilon_r + 1}{2} + \frac{\epsilon_r - 1}{2} \left[\frac{1}{\sqrt{1 + 12 \left(\frac{h}{w}\right)}} \right] \quad (2)$$

Step 3: The extension length of EM (ΔL): calculation

$$\frac{\Delta L}{h} = 0.412 \frac{(\epsilon_{\text{reff}} + 0.3) \left(\frac{w}{h} + 0.264\right)}{(\epsilon_{\text{reff}} - 0.3) \left(\frac{w}{h} + 0.8\right)} \quad (3)$$

Step 4: Fabricated length of patch (L) Calculation

$$L = \frac{C_0}{2f_r \sqrt{\epsilon_{\text{eff}}}} - 2\Delta L \quad (4)$$

Step 5: The microstrip patch antenna (L_p) length

$$L_p = L + 2\Delta L \quad (5)$$

Step 6: Position of inset feed point (Y_0) calculation

$$Y_0 = \frac{L}{\pi} \cos^{-1} \left(\sqrt{\frac{Z_{\text{in}}}{R_{\text{in}}}} \right) \quad (6)$$

Step 7: Ground dimensions (W_g & L_g) calculation

$$W_g = 6H + W_p \quad (7)$$

$$L_g = 6H + L_p \quad (8)$$

Step 8: Calculation of characteristic impedance (Z_0):

In this step, we have two cases:

1. $\frac{w}{h} < 1$

$$Z_0 = \frac{138}{\sqrt{\epsilon_{\text{reff}}}} \ln \left(8 \frac{h}{w} + \frac{w}{h} \right) \quad \Omega \quad (9)$$

2. $\frac{w}{h} > 1$

$$Z_0 = \frac{120\pi}{\sqrt{\epsilon_{\text{reff}} \ln \left(\frac{w}{h} + 1.393 + 1.536 \ln \left(\frac{w}{h} + 1.444 \right) \right)}} \quad \Omega \quad (10)$$

Step 9: Calculations of phase velocity (v_p):

$$v_p = \frac{c}{\sqrt{\epsilon_{\text{reff}}}} \quad \text{m/s} \quad (11)$$

The speed of waves that go through the antenna cannot be assumed to be "c" nor (c/λ), for the propagation partially goes through the substrate and partially through the air, so it's a mixture of both. Therefore, the effective permittivity is used to calculate the phase velocity.

Step 10: Calculation of attenuation (α):

Attenuation in a microstrip line is a function of dielectric properties, conductivity, and geometry of the antenna; mainly, we have two types of attenuation:

1. Dielectric attenuation (α_d)

$$\alpha_d = 377 \frac{\sigma_d}{2} \sqrt{\frac{\mu_r}{\epsilon_r}} \quad \text{NP/m} \quad (12)$$

2. Conductor attenuation (α_c)

$$\alpha_c = \frac{1}{Z_0 W_0} \sqrt{\frac{\pi f_r \mu_0}{\sigma_c}} \quad \text{NP/m} \quad (13)$$

And

$$\alpha_{\text{total}} = \alpha_d + \alpha_c \quad \text{NP/m} \quad (14)$$

Step 11: Calculation of quality factor (Q):

The quality factor is the ratio between stored and lost energy; this determines the efficiency of an antenna.

$$Q = \frac{\beta}{2\alpha} \tag{15}$$

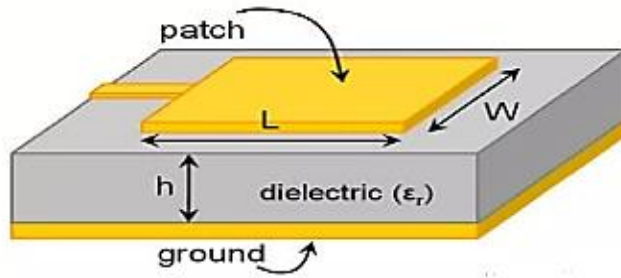


Fig. 1: Design of patch antenna.

Use all this information and equations to get the SIW antenna geometry figure.2:

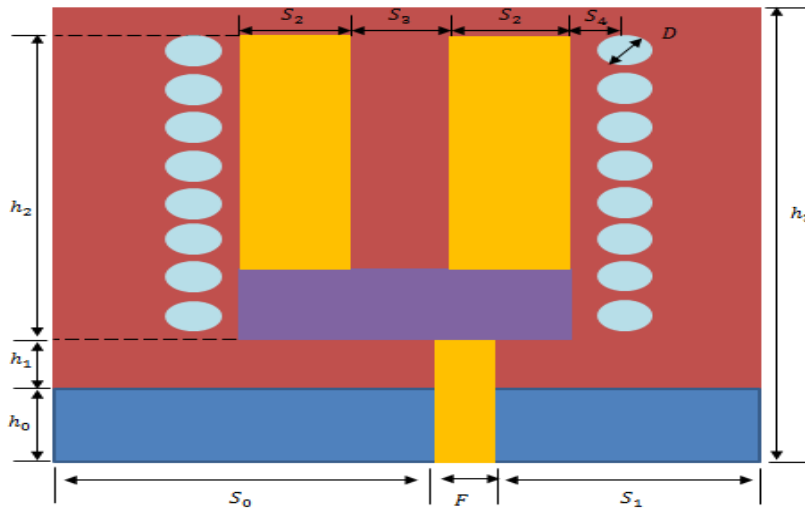


Fig. 2: SIW with one array hole.

A dielectric substrate of FR4-Epoxy, $\epsilon_r = 4.4$, $\tan(\delta) = 10^{-3}$, and thickness $t = 0.8$ mm has been considered.

Table. 1: The geometric antenna characteristics acquired post the optimization process.

parameter	S_0	S_1	S_2	S_3	S_4	h_0	h_1	h_2	h_3	D	F	d
(mm)	15.8	11.09	5	3	1.75	7.55	0.6	18.8	30	1.5	1.91	2.51

In our project, the effect of adding array holes on bandwidth (S11) and SWR was discussed. Four antennas were designed (without holes, one array hole, two holes, and three holes), with varied distances between the centers of array holes (d).

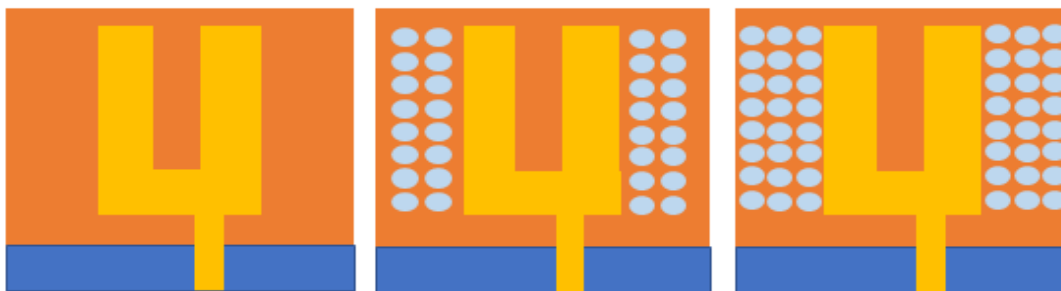


Fig. 3: (a) SIW without array hole, (b) SIW with two array hole, (c) SIW with three array hole

MATLAB code is employed to simulate and compute the dimensions of the patch antenna.

2 The experimental and practical part

After all these calculations, we sent all dimensions in SAB files to the National Telecom Nation Institute (NTI) for fabrication and simulation.

Initially, the fabrication process involved the following steps:

1. Metallization of copper vias.
2. Fabrication of the original antenna via CNC milling.
3. Dry film lamination.
4. Taking off the protective sheet also means removing the dry film covering the holes.
5. evaporation of the Copper.
6. Removal of dry film.
7. Observation of hole metallization from the bottom side of the antenna.

After layering, the front side was heated to 120°C for one minute to improve the dry film's adherence. After cooling, the dry film's protective layer and the dry film covering the holes were removed. After that, the antenna prototype was firmly attached to a 6-inch silicon wafer using adhesive Kapton tape and put inside an evaporation chamber. Next, an e-gun evaporation process was used to deposit a nominally 1.5 μm thick copper layer at ambient temperature and vacuum. The antennas were removed from the support and immersed in a 10% KOH solution to remove the copper layer above the dry film during lift-off. Comparing SIW configurations with one, two, or three array holes—or even without holes—is analogous to evaluating Egyptian pounds in images of the antenna prototype's top and bottom sides. With a sub-miniature type (SMA) coaxial connector installed, the approximate dimensions can be determined by looking at the images in Figures 4 and 5.

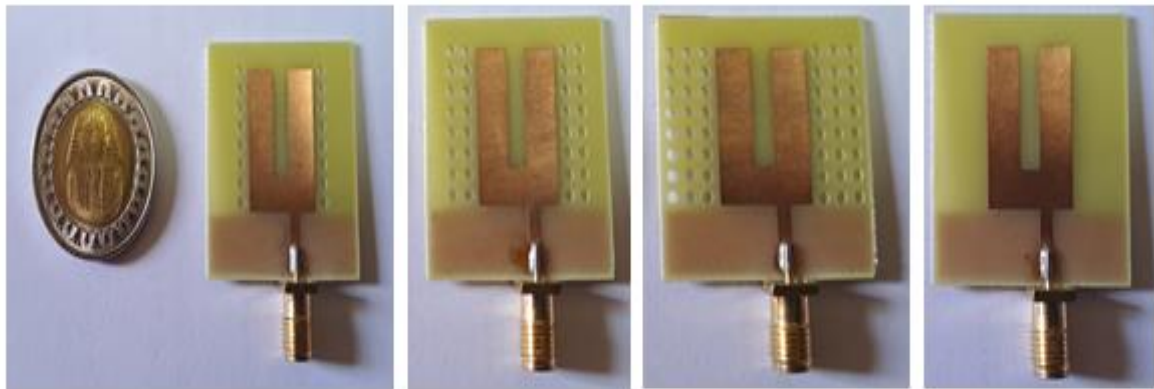


Fig. 4: Top view of the SIW antennas.

Second, using (VNA) to get the value of S11 and SWR.

The simulation files were sent to the National Telecommunication Institute (NTI) for fabrication, where identical materials—Copper sheet for the conductor and FR4 Epoxy for the substrate—were used, ensuring adherence to specified dimensions as closely as possible. Each antenna was equipped with a sub-miniature type (SMA) coaxial connector, as depicted in Figure 6. Post-fabrication, the connector was securely attached to each antenna as the coaxial input connector. Following this, the antennas were transferred to the measurement and testing lab to compare actual measurements with theoretical ones. The S11 and SWR values of the four antennas were meticulously recorded and measured utilizing a vector network analyzer (VNA). The VNA was set to default configurations, with the bandwidth set from 2GHz to the maximum limit of 18GHz. The recorded values were then saved in Microsoft Excel sheet format for further analysis. A comprehensive comparison was facilitated by importing the recorded values into MATLAB, where they were utilized to generate plots and directly compare them with the HFSS values. The ensuing comparison is illustrated in the subsequent figures.

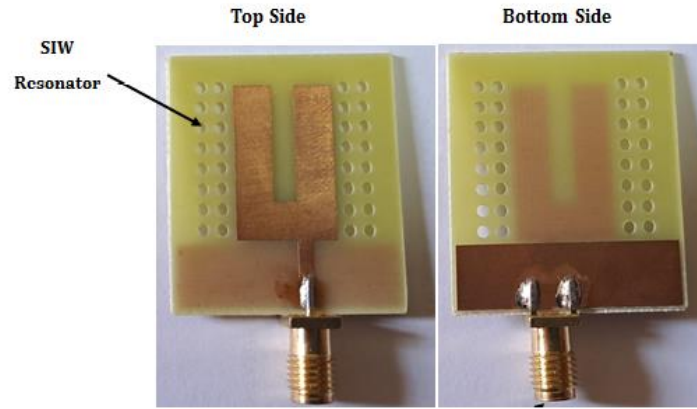


Fig. 6: Coaxial Connector.

The S_{11} and SWR of the antenna were measured using a Vector Network Analyzer (VNA), as illustrated in Figure 7. Measurements were also taken on an antenna prototype that lacked the SIW structure to evaluate the effect of the SIW cavity. The prototype's S_{11} with the SIW cavity (shown by the green dotted line) satisfies the original requirements. Over the whole frequency range under consideration, the return loss is far less than the initial requirements, roughly 10 dB.

Figures 3 and 4 delineate the reference level by the dotted black line, serving as a benchmark against which measurements are compared. Numerical data collected using the ADS commercial program has been juxtaposed with the experimental measurements to facilitate easier comparison. The results exhibit a notably commendable alignment between the numerical simulations and the empirical data. However, upon closer examination, an anomaly becomes apparent within the numerical data near the frequency of $f = 2.8$ GHz. This peculiar peak is conspicuous within the numerical results but is conspicuously absent from the corresponding experimental readings.

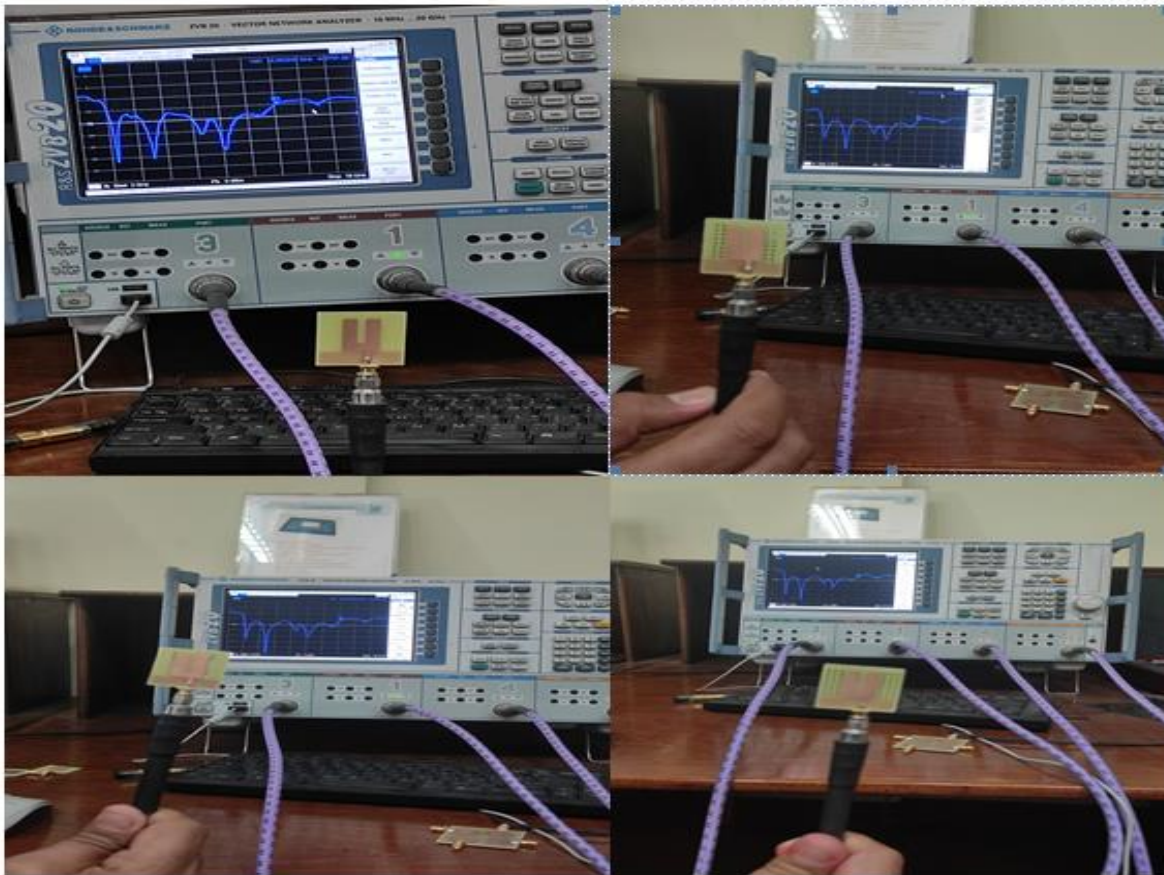


Fig. 7: The antenna S_{11} and SWR have been measured by Vector Network Analyzer (VNA).

Third, the output results from VNA reads S11 and SWR for 4 array antennae are shown in the following figures.

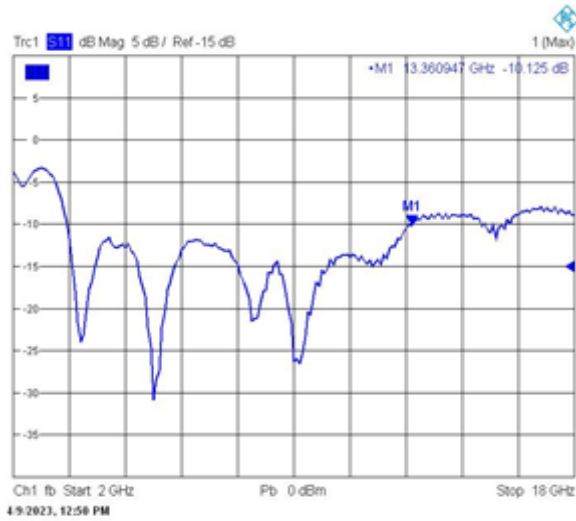


Fig. 8: Measuring the S11 of the zero-hole antenna.

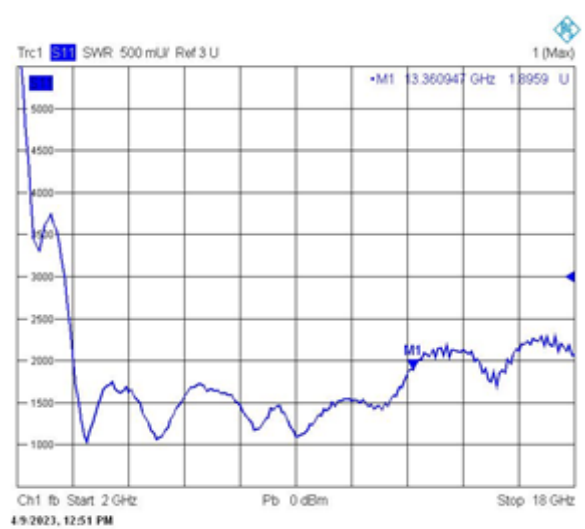


Fig. 9: Measuring the SWR of the zero-hole antenna

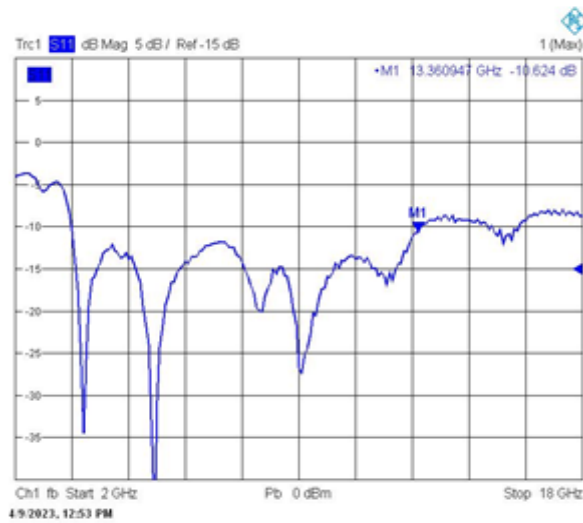


Fig. 10: Measuring the S11 of the one-hole antenna.

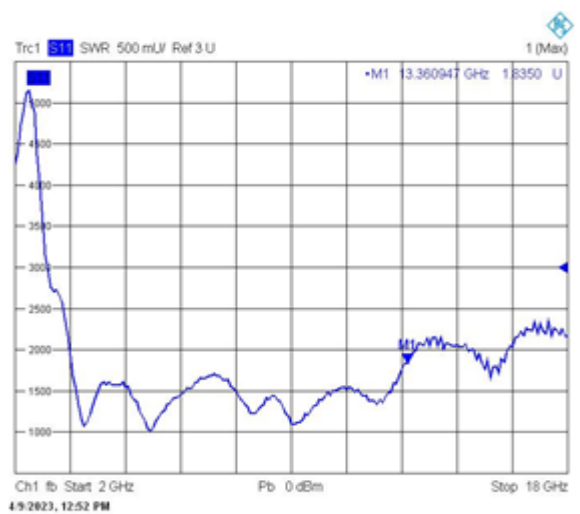


Fig. 11: Measuring the SWR of the one-hole antenna.

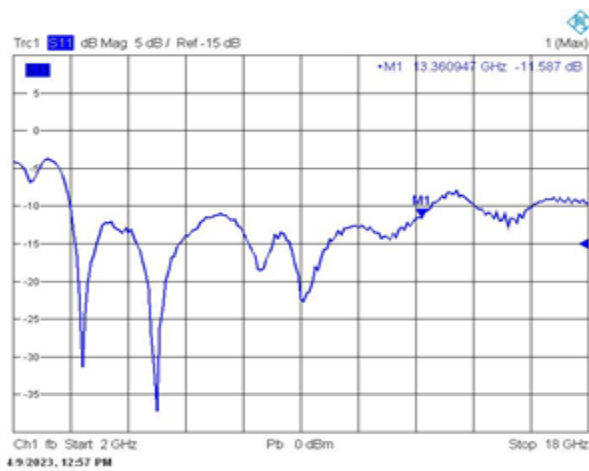


Fig. 14: Measuring the S11 of the three-hole antenna.

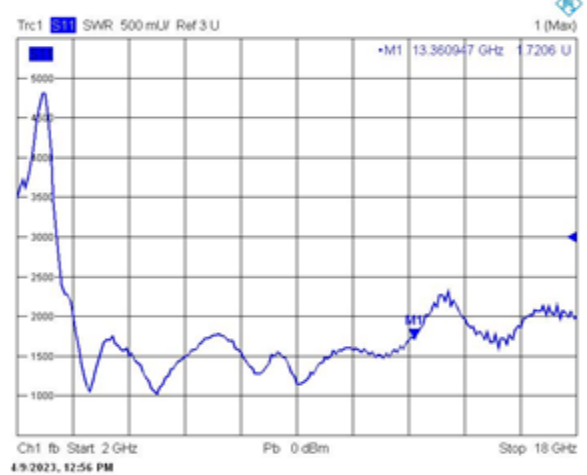


Fig. 15: Measuring the SWR of the three-hole antenna

Table 2: Results of the Designed antennas.

	No hole	One	Two	Three
Bandwidth (GHz)	9.86	9.9	10.1	9.85
S₁₁ (dB)	-31.2	-47.5	-27.5	-39.86
VSWR	1.06	1.07	1.097	1.039

3 Results and Simulations

The process involved importing the data extracted from the Excel sheet into MATLAB, which was processed and visualized to highlight the disparities among the antennas under scrutiny. Figure 16 was generated to showcase the S₁₁ characteristics of all antennas, offering a comprehensive view of their respective performance regarding reflection coefficient. Similarly, Figure 17 was created to depict the Voltage Standing Wave Ratio (VSWR) across the frequency range of interest, providing insights into the impedance-matching capabilities of the antennas.

Following the visualization stage, the simulation and output steps were presented systematically to enable a detailed comparison between them. This involved demonstrating how the simulated results align or deviate from the actual measured data, shedding light on the accuracy and reliability of the simulation model. A thorough understanding of the antenna behavior and performance characteristics was attained by juxtaposing the simulation outputs with the empirical measurements, facilitating informed decision-making and potential design refinement.

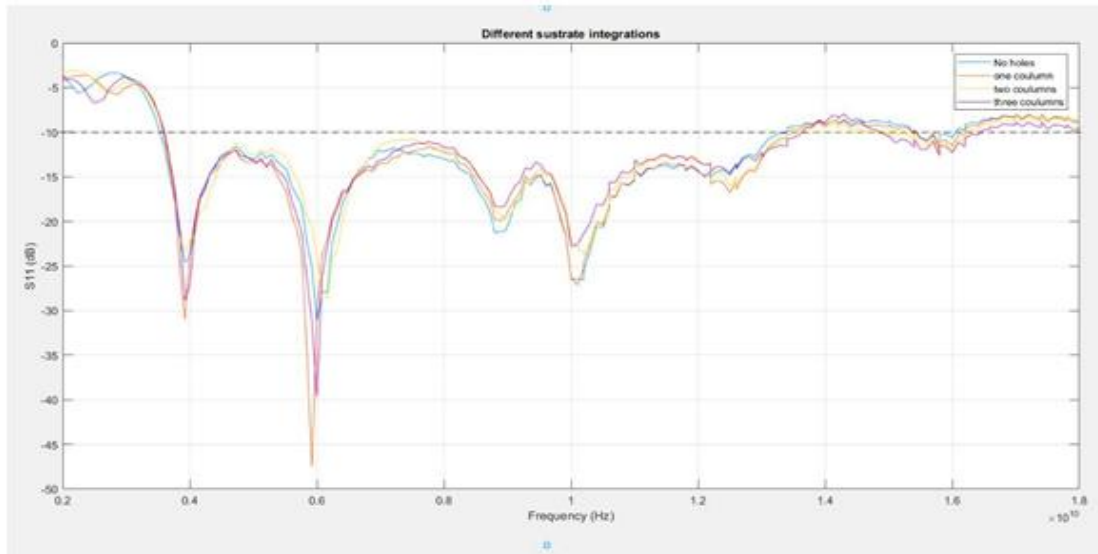


Fig. 16: Excel sheet S₁₁ plot of all the antennas.

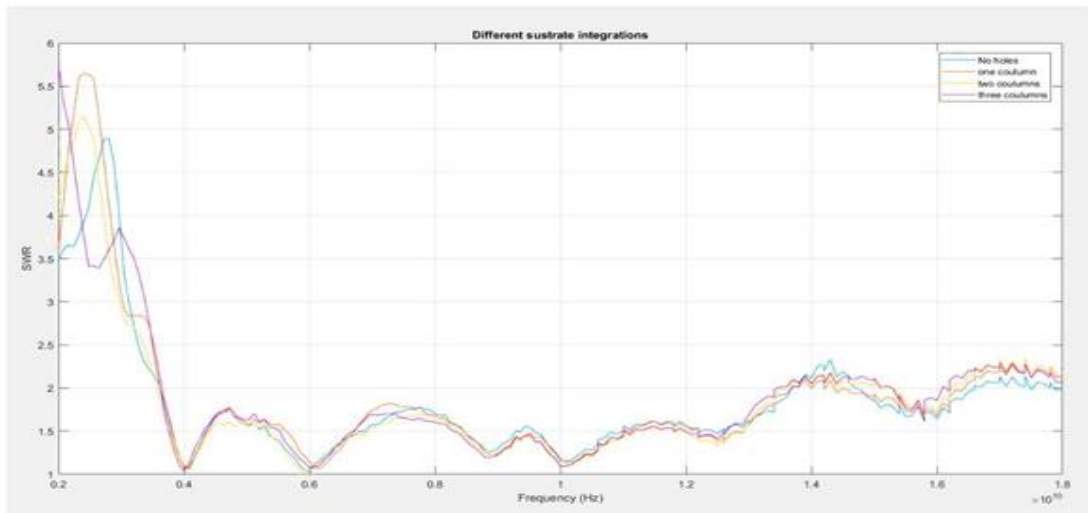


Fig. 17: Excel sheet SWR plot of all the antennas.

Before fabricating the antenna, we need to know the best length of ground that we will use, so the open HFSS simulation and testing phase is to compare different ground lengths (complete, half, and quarter) and see how it alters the characteristics and values of bandwidth, S11 (dB, at peak), Gain (dB) and VSWR.

Table 3: shows an overall comparison between the ground lengths.

Comparison	Ground Length	Full	Half	Quarter
Bandwidth		~0.5GHZ	0.7893GHz	13.4GHz
S ₁₁ (dB, at peak)		-27.5	-14.5	-30
Gain (dB)		-2.8645	1.8534	4.2750
VSWR		0.28	0.34	0.29

Following the thorough comparison between the different antenna configurations, it becomes evident that the quarter ground configuration emerges as the superior choice, displaying significantly better results across various performance metrics. The quarter ground configuration not only outperforms other designs by a substantial margin but also exhibits promising characteristics that could serve as a solid foundation for further exploration, particularly in the context of Substrate Integrated Waveguide (SIW) applications. Because of extensive benefits, it has been decided to make this last antenna prototype for the quarter ground, the final reserved position. This decision might be due to an exceptional performance by the product, which appears to be the one that can provide the requirements and targets with high effect.

The last antenna design – the chip effect – is brought to action and was prepared for field tests and evaluation. The figures below show the results obtained for the four antenna arrays in the following figures, and the comparison is very comprehensive. The simulation results of all the cases prove that the quarter ground configuration is the primary candidate that shows the most insightful performance characteristics of the morphing directional antennas.

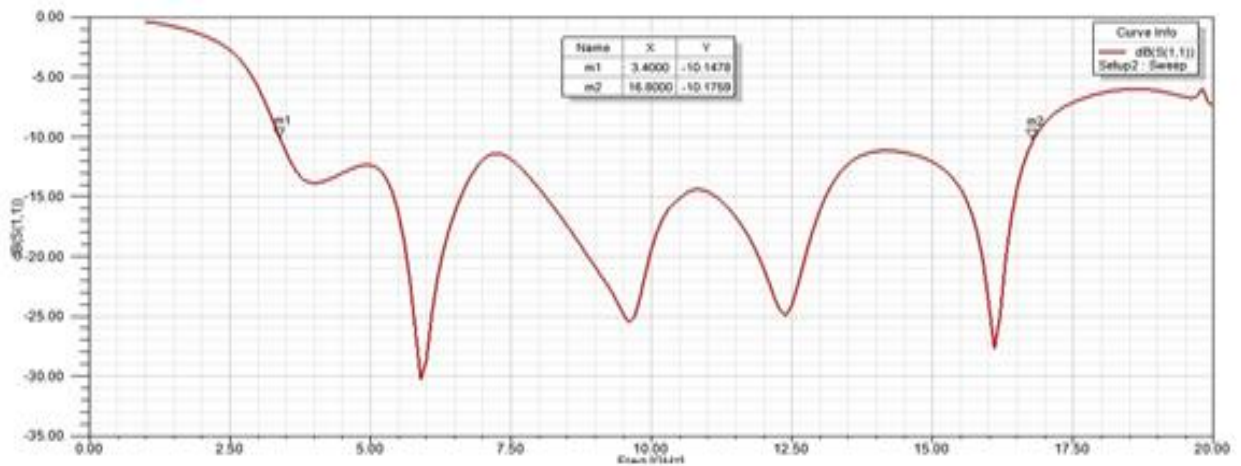


Fig. 18: Return loss S₁₁ (dB) of normal microstrip Antenna "Without holes."

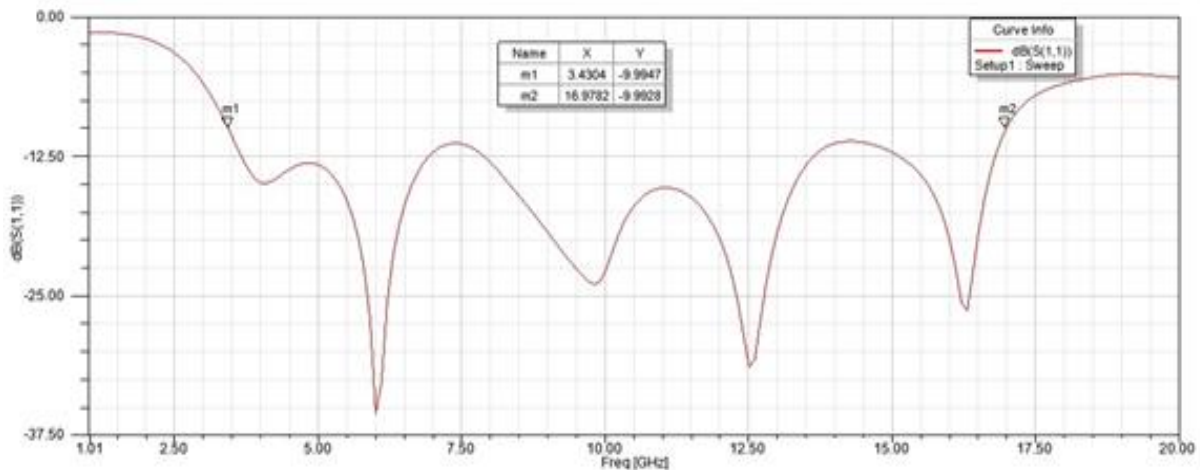


Fig. 19: Return loss S₁₁ (dB) of SIW with one array of holes.

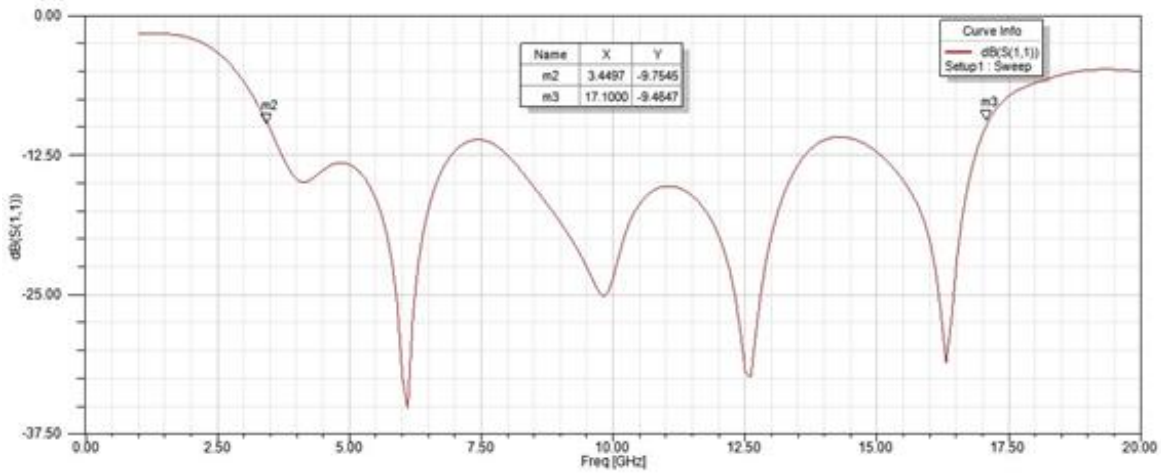


Fig. 20: Return loss S_{11} (dB) of SIW with two array holes.

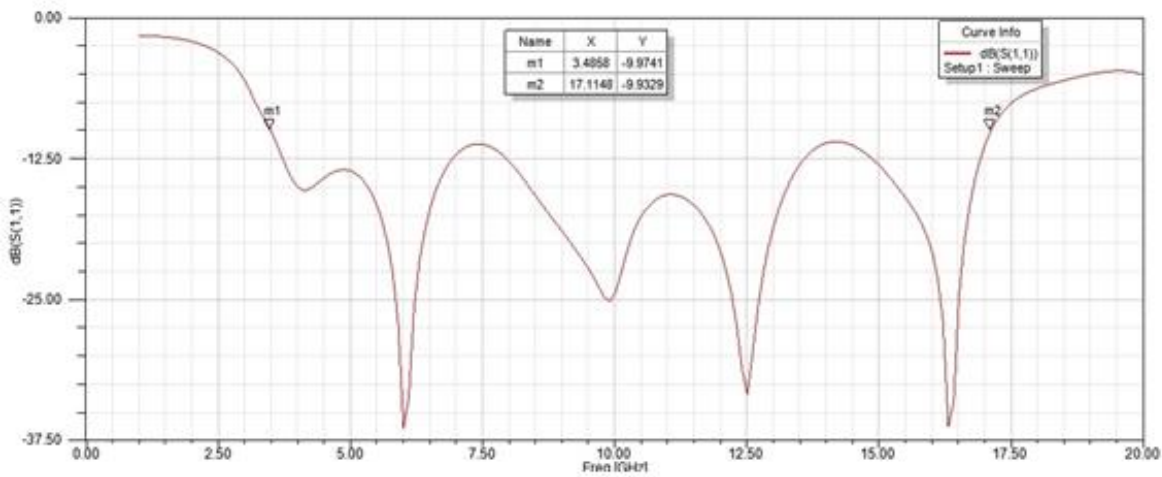


Fig. 21: Return loss S_{11} (dB) of SIW with three array holes.

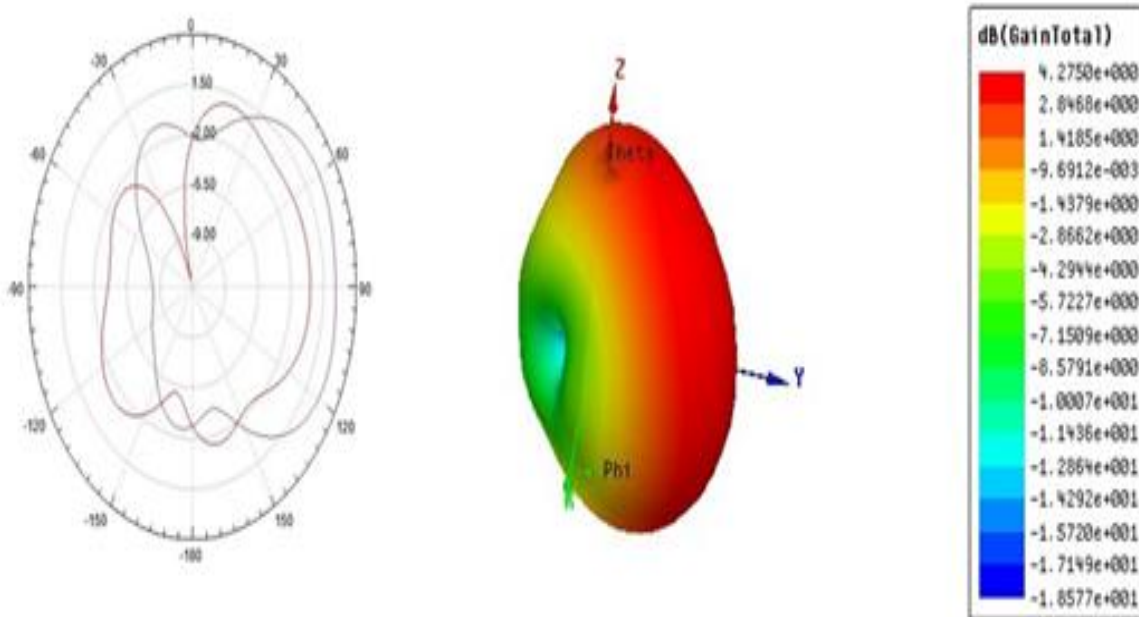


Fig. 22: Gain 3D Polar Plot & Radiation Pattern of normal microstrip Antenna "Without holes".

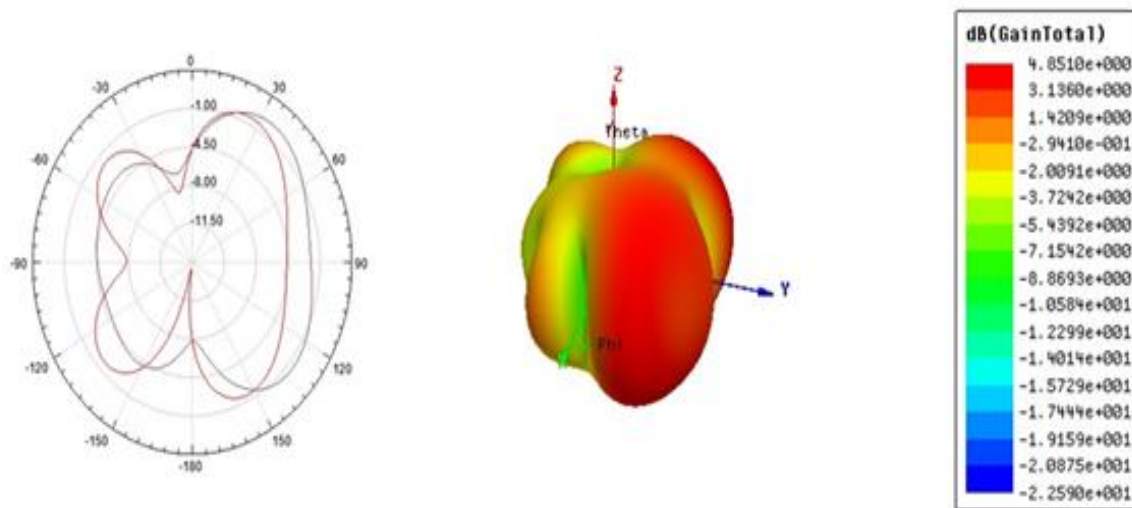


Fig. 23: Gain 3D Polar Plot & Radiation Pattern of SIW with one array holes.

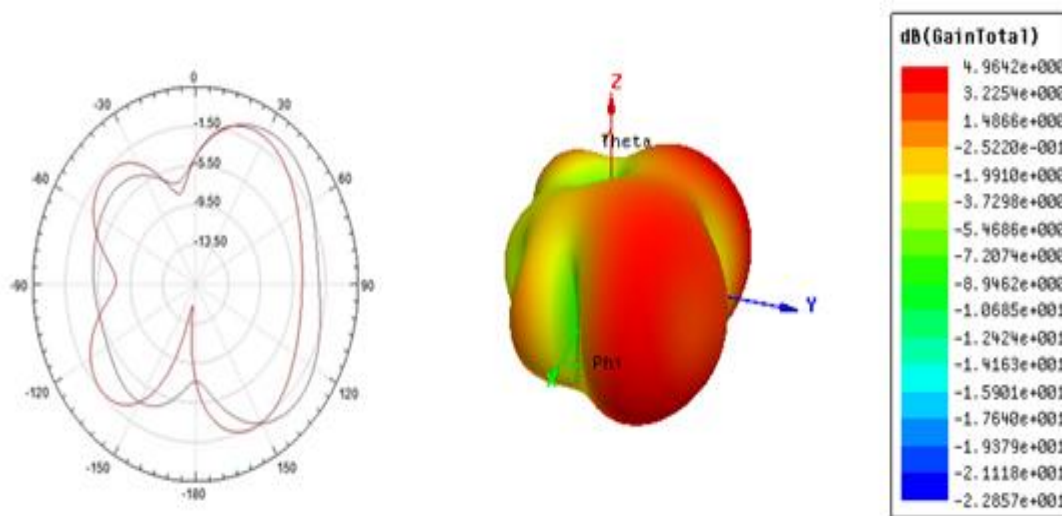


Fig. 24: Gain 3D Polar Plot & Radiation Pattern of SIW with two array holes.

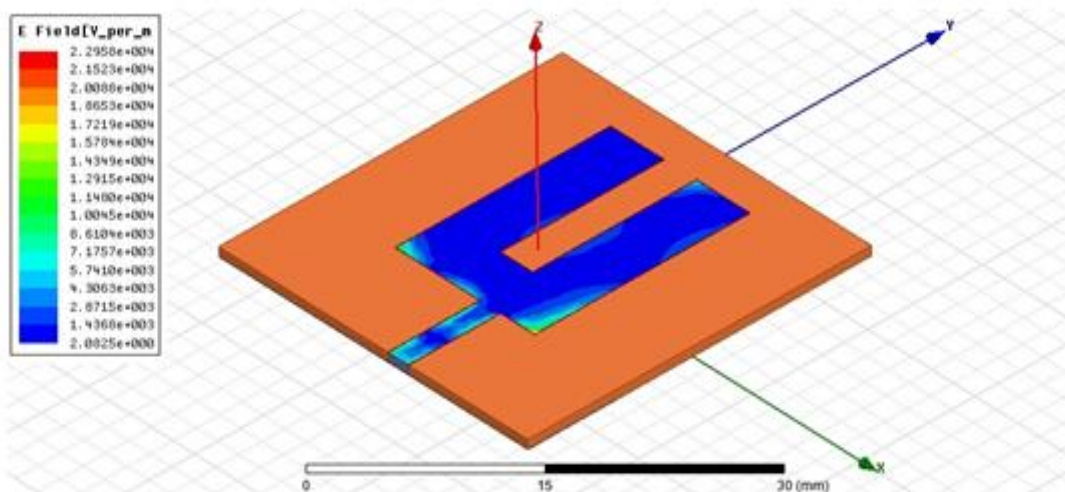


Fig. 25: Electromagnetic radiation pattern of normal microstrip Antenna "Without holes".

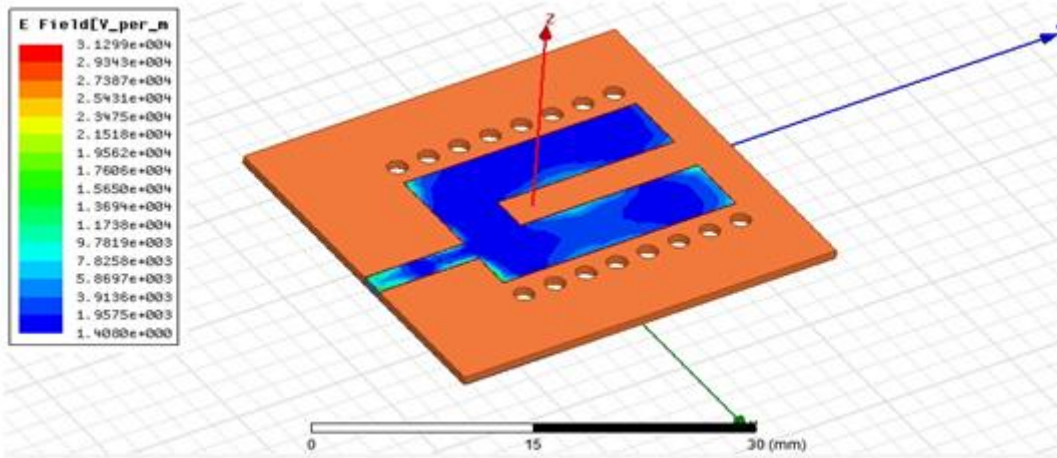


Fig. 26: Electromagnetic radiation pattern of SIW with one array of holes.

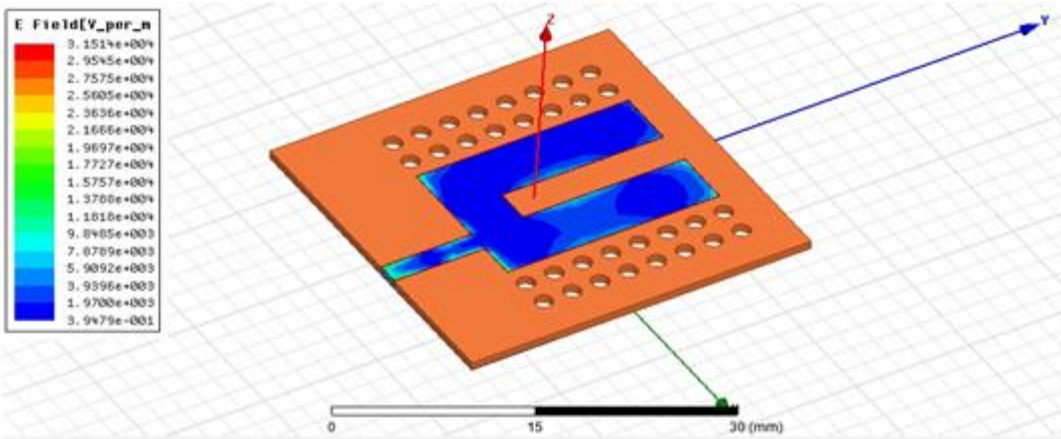


Fig. 27: Electromagnetic radiation pattern of SIW with two array holes

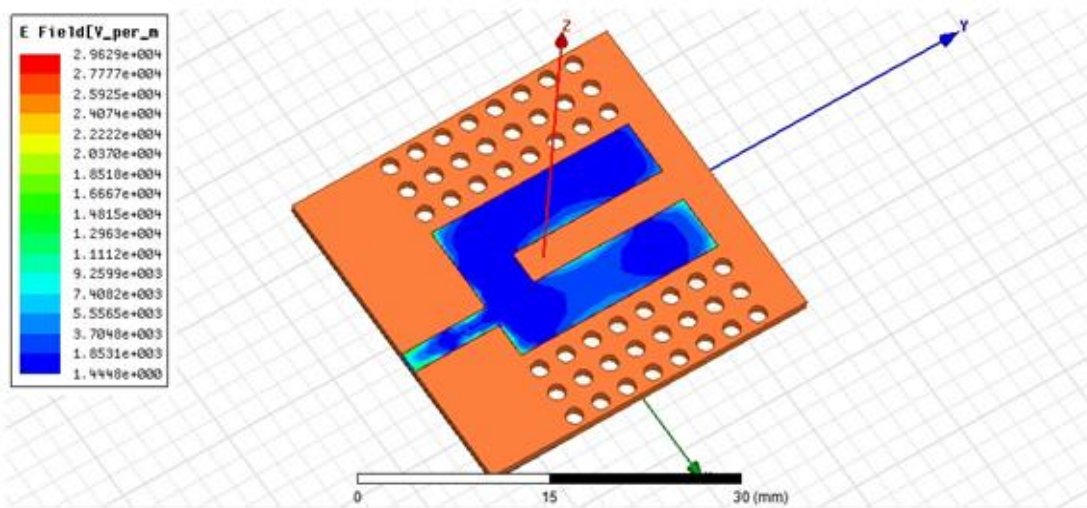


Fig. 28: Electromagnetic radiation pattern of SIW with three array holes.

Table 4: compares the three integrations and the regular patch for a more thorough comparison.

Comparison	Integration	Without Holes	One Array Holes	Two Array Holes	Three Array Holes
BW (GHz)		13.4	13.5478	13.6503	13.629
S₁₁ (dB, at peak)		-30	-35	-35	-37

Gain (dB)	4.275	4.851	4.9642	4.9258
Directivity (dB)	9.185	5.504	5.534	5.540
E-Field (V/m)	2.295×10^4	3.1299×10^4	3.1514×10^4	2.9629×10^4
H-Field (A/m)	1.239×10^2	2.235×10^2	2.213×10^2	2.235×10^2
VSWR	0.29	0.13	0.19	0.19
Radiation efficiency (%)	18.03	87.43	87.69	87.66

In the final comparison, it becomes apparent that some added features significantly contribute to the antenna's quality level and help realize the idea of the UWB antenna. The standout measures from the results are the ones with improved VSWR and gain. This demonstrates superiority over the traditional conductor patch antenna. This fact illustrates how effective SIW-aided patch antenna is towards improving the general performance characteristics of the conventional antenna. By contrast with the cumulative results, we can safely say that the antenna with two holes columns is the best one since it is the most precise compared to the set objectives. The indicators signify a higher performance rate for this setup, making it effective and efficient in achieving its goals. The after-integration study is conducted when researchers compare the four types of antennas from the perspective of real-life situations. Hence, testing the developed antennas shall be performed to determine their real potential and ensure the correctness of the simulation result. These tests will thus offer factual evidence showing how the antenna works in the real environment, allowing for future adjustments and improvement.

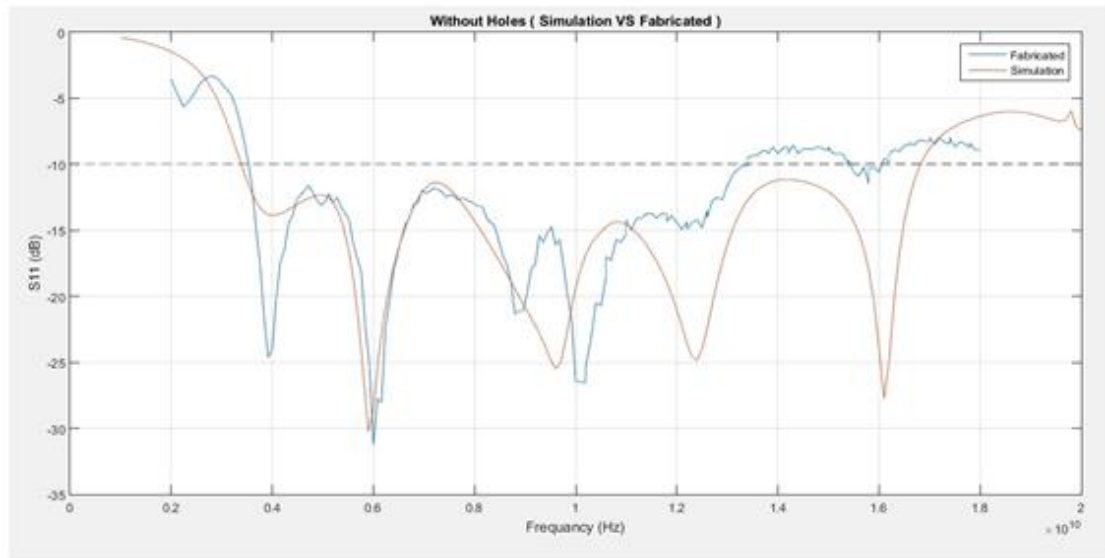


Fig. 29: Without holes (Simulation VS Fabricated).

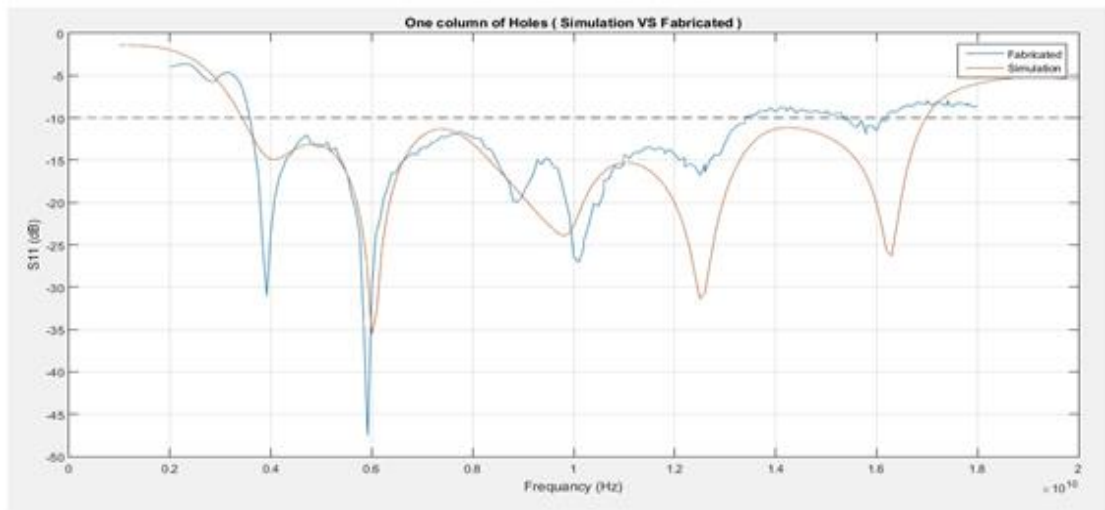


Fig. 30: One array holes (Simulation VS Fabricated).

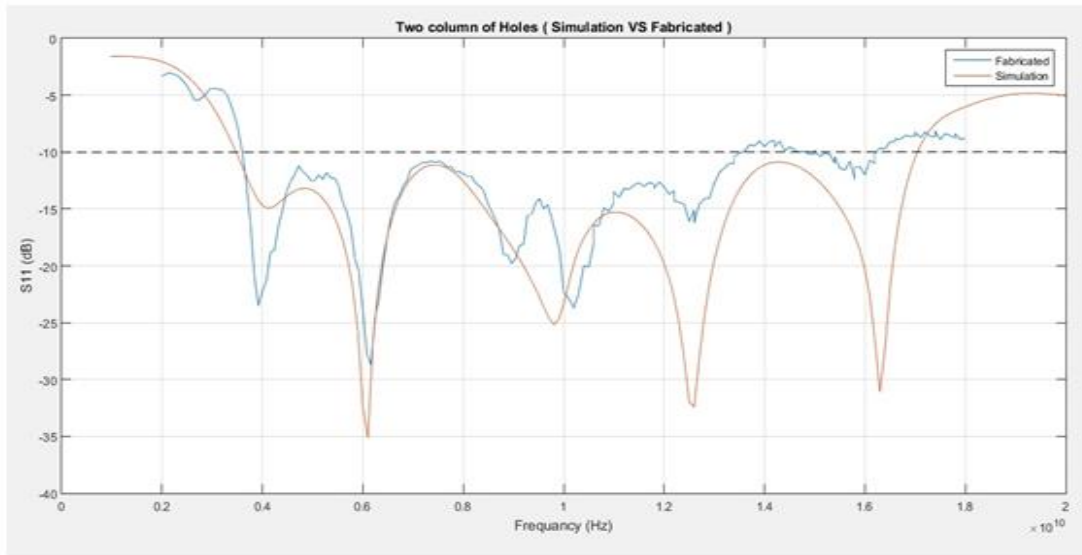


Fig. 31: Two array holes (Simulation VS Fabricated).

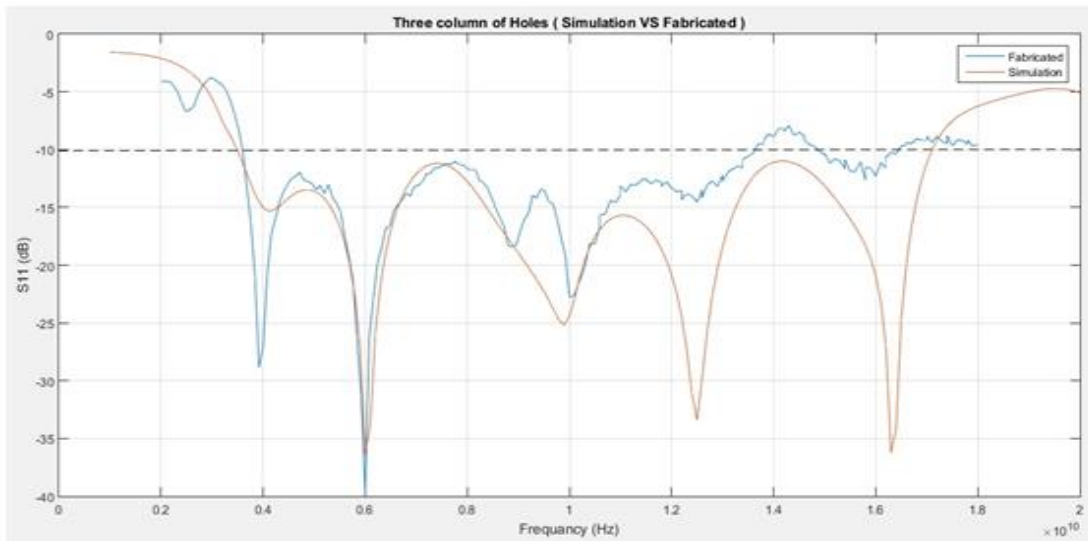


Fig. 32: Three array holes (Simulation VS Fabricated).

A complete comparison of the four antenna types between the actual "Real" value and the Simulation value is shown in Table 5, based on the discussion and analysis conducted. Some apparent differences between the simulated and measured results can be observed; these differences could be attributed to manufacturing or measurement phase errors or simply to real-world effects of electromagnetic energy on the antenna.

5 Conclusions

	Zero Hols		One Column		Two Columns		Three Columns	
	Sim	Real	Sim	Real	Sim	Real	Sim	Real
Bandwidth (GHz)	13.4	9.86	13.5478	9.9	13.6503	10.1	13.629	9.85
S₁₁ (dB)	-30	31.2	-35	-47.5	-35	-27.5	-37	-39.86
VSWR	0.29	1.06	0.13	1.07	0.19	1.097	0.19	1.039

Wireless communication between devices has become a necessity, and it is growing at an exponentially fast rate; this growth cannot be satisfied by the conventional bulky antenna because of its size, cost, and production time; the demands have to be met by a cheap, smaller, easy to install and replaceable antenna, with the help of PCB technology, the patch antenna is created and it seems to be a suitable replacement for the traditional antenna for it meets all the

requirements for the wireless communication advancement, it has a reasonable gain radiation, good S11 values, good VSWR, and low reflection coefficient so, it could be applied for a wide variety of applications; mobile devices, IoT, data gathering and machine learning, satellite communication, and energy harvesting. There was a significant problem with the patch antenna; the bandwidth of the regular patch antenna is relatively narrow, and in this type of application, it is preferred that the antenna can receive as much electromagnetic energy as possible, so the antenna has to have a bandwidth in the UWB range which means that it can operate at a frequency range of more than 500MHz. To achieve this target, we have to use the substrate-integrated waveguide method, where we, as the name suggests, change the structure of the substrate layer of the antenna by removing or adding parts depending on the target. For the target of broadening the bandwidth, we concluded that adding arrays (columns) of holes that go through the entire antenna on each side of the patch achieves this goal perfectly. To lay a good foundation for the integrations, we tested multiple shapes for the base antenna to see which one acquired the parameters closer to the desired goal and concluded that the fork shape with the quarter ground of length was the best. The materials chosen for the antenna are copper for the conductors and FR4 epoxy for the substrate at a thickness of 0.8mm, and a coaxial connector is used for input/output. Three integrations were tested: one column, two columns, and three columns of holes along with the regular antenna. The tests were done using HFSS software, the exact dimensions and materials were applied, and the following parameters (S11, VSWR, gain, directivity, electric field, and magnetic field) were tested and plotted along with the radiation efficiency. In conclusion, the integrations do improve the characteristics of the antenna; and the two columns of holes generated the best results among all integrations. However, to test the accuracy of the simulated results, all antennas that include the regular fork patch were sent for manufacturing. The simulation files were sent to the NTI for manufacturing and testing. After the measurement using VNA, we noticed that the simulation results had some slight differences; this could be due to errors in the manufacturing, measuring or simply due to real-world effects on the electromagnetic radiation characteristics on the antenna.

References

- [1] D.M. Pozar, *Microwave Engineering*, 4th Edition, John Wiley & Sons.
- [2] Mao, Chun-Xu, et al. Multimode resonator-fed dual-polarized antenna array with enhanced bandwidth and selectivity. *IEEE Transactions on Antennas and Propagation*, 2015, 63.12: 5492-5499.
- [3] Bhalla, Devan; Bansal, Krishan. Design of a rectangular microstrip patch antenna using the inset feed technique. *IOSR Journal of Electronics and Communication Engineering*, 2013, 7.4: 08-13.
- [4] Arun, V.; Reddy, N. Vasu Deva; Reddy, G. Sridhar. Design of Polarized Rectangular Microstrip Patch Antenna.
- [5] Howell, J. Microstrip antennas. *IEEE Transactions on Antennas and Propagation*, 1975, 23.1: 90-93.
- [6] Breed, Gary, et al. The fundamentals of patch antenna design and performance. *High frequency electronics*, 2009, 3.12: 49-51.
- [7] Chen, Pai-Yen, et al. Flatland plasmonics and nanophotonics based on graphene and beyond. *Nanophotonics*, 2017, 6.6: 1239-1262.
- [8] Ramachandran, Siddharth, et al. Ultra-large effective-area, higher-order mode fibers: a new strategy for high-power lasers. *Laser & Photonics Reviews*, 2008, 2.6: 429-448.
- [9] Caytan, O., et al., "Half-mode substrate-integrated-waveguide cavity- backed slot antenna on cork substrate," *IEEE Antennas Wireless Propag. Lett.*, Vol. 15, 162–165, 2016.
- [10] Donelli, M., "A chipless RFID system based on substrate impedance waveguide resonators (SIW)," *IEEE-APS Topical Conference on Antennas and Propagation in Wireless Communications (APWC)*, IEEE, Proceedings of: IEEE-APS, 29–32, Verona, Italy, Sept. 11–15, 2017.
- [11] Matin, M. A.; Sayeed, A. I. A design rule for inset-fed rectangular microstrip patch antenna. *WSEAS Transactions on Communications*, 2010, 9.1: 63-72.
- [12] Anand, S.; Prashalee, P. High gain compact multiband cavity backed SIW and metamaterial unit cells with CPW feed antenna for S, and Ku band applications. *Wireless Personal Communications*, 2021, 118.2: 1621-1634.
- [13] Hammu-Mohamed, Bilal, et al. SIW cavity-backed antenna array based on double slots for mmWave communications. *Applied Sciences*, 2021, 11.11: 4824.
- [14] Zelenchuk, Dmitry E., et al. Millimeter-wave printed circuit board characterization using substrate integrated waveguide resonators. *IEEE Transactions on Microwave Theory and Techniques*, 2012, 60.10: 3300-3308.

- [15] Shaik, L. A., C. Saha, J. Y. Siddiqui, et al., "Ultra-wideband monopole antenna for multiband and wideband frequency notch and narrowband applications," *IET Microw. Antennas Propag.*
- [16] Tang, Z., R. Lian, and Y. Yin, "Differential-fed UWB patch antenna with triple band-notched characteristics," *Electron. Lett.*, Vol. 51, No. 22, 1728–1730, 2015.
- [17] Hung, W.-P., et al., "Non-invasive detection of object by UWB radar," 2017 Asia-Pacific International Symposium on Electromagnetic Compatibility (APEMC), IEEE, 16971, 2017.
- [18] Wu, S., et al., "Person-specific heart rate estimation with ultra-wideband radar using convolutional neural networks," *IEEE Access*, Vol. 7, 16848494, 2019.
- [19] Shehata, M., M. S. Said, and H. Mostafa, "Dual notched band quad-element MIMO antenna with multitone interference suppression for IR-UWB wireless applications," *IEEE Trans. on Antennas Propagat.*, Vol. 66, No. 11, 5737–5746, Nov. 2018.
- [20] Cai, Y.-Z., H.-C. Yang, and L.-Y. Cai, "Wideband monopole antenna with three band-notched characteristics," *IEEE Antennas Wireless Propag. Lett.*, Vol. 13, 607–610, 2014.
- [21] Reddy, G. S., A. Kamma, and J. Mukherjee, "Compact printed monopole UWB antenna loaded with non-concentric open-ended rings for triple band-Notch characteristic," *Proceeding in Proc. APMC*, 221–223, Seoul, South Korea, Nov. 2013.
- [22] Tang, T.-C. and K.-H. Lin, "An ultrawideband MIMO antenna with dual band-notched function," *IEEE Antennas Wirel. Propag. Lett.*, Vol. 13, 1076–1079, 2014.